Supporting Information

Two-Dimensional Viologen-Based Lanthanide Coordination Polymers as Multi-Stimuli Responsive Materials to Light, Amine, and Fluorescence Response

Hao Wang, Xiao-Han Sun, Tian-Tian Wang, Yu-Xin Li, Ying-Ming Xu, Wen-Bin Sun*

Key Laboratory of Functional Inorganic Material Chemistry Ministry of Education, School of Chemistry and Material Science Heilongjiang University, 74 Xuefu Road, Harbin 150080, P. R. China.

*E-mail: wenbinsun@126.com

Experimental section

Materials and reagents

All reagents and solvents were purchased commercially and used without further purification.

Synthesis of N, N′-4,4′-Bipyridinio-dipropionate ($H_2BpydpCl_2$)

The N, N′-4,4′-Bipyridinio-dipropionate ligand was synthesized according to previously reported methods.[1, 2]

Synthesis of [(Bpydp)Eu(H_2O)(BDC)]·NO_3·2H_2O (1)

A mixture of 0.1 mmol (37.2 mg) of $H_2Bpydp·2Cl$, 0.1 mmol (16.6 mg) of H_2BDC, 0.1 mmol (44.6 mg) of $Eu(NO_3)_3·6H_2O$, 4 mL ethanol, 2 mL N, N-dimethylformamide, and 2 mL H_2O in a closed 25 mL Teflon-lined autoclave was heated at 80 ℃ for 72 h and then cooled to room temperature naturally. Faint yellow rod-shaped crystals were collected by filtration, and the yield was 48 % (based on Eu^{III}). Selected IR (KBr, cm^{-1}): 3420(w), 3067(w), 2670(w), 2545(w), 1681 (w), 1574(s), 1504(m), 1383(s), 1309(w), 1015(w), 953(w), 883(m), 827(m), 754(m), 673(w), 570(w). Elemental analysis: (wt %) calcd for $C_{24}H_{30}EuN_3O_{14}$: C, 39.14; H, 4.11; N, 5.71. Found: C, 39.31; H, 4.22; N, 5.69.

Synthesis of [(Bpydp)Tb(H_2O)(BDC)]·NO_3·2H_2O (2)

Synthesized as above, $Tb(NO_3)_3·6H_2O$ (45.3 mg, 0.1 mmol). Faint yellow rod-shaped crystals, yield: 36%. Selected IR (KBr, cm^{-1}): 3375(w), 3013(w), 2671(w), 2537(w), 1606(s), 1448(m) 1377(s), 1315(w), 1152(w), 954(w), 887(m), 826(m), 756(m), 672(w), 566(m).Elemental analysis: (wt %) calcd for $C_{24}H_{30}TbN_3O_{14}$: C, 39.35; H, 3.96; N, 5.74. Found: C, 39.46; H, 4.12; N, 5.79.

Crystal structure determination

Single-crystal X-ray diffraction was performed on all complex crystals. Space group, unit cell dimensions, and intensity data were measured with an Xcalibur Eos diffractometer at 293/150 K using Cu Kα radiation (λ = 1.54184 Å). Absorption corrections were applied using the multi-scan method. Structures were resolved directly with intrinsic phasing in SHELXT (Sheldrick) and analyzed using Olex2. [3-5]All crystallographic data for complexes **1** and **2** are summarized in Table

S1. The results are included in the CIF (CCDC 2355401(**1**) 2355402(**2**)). The free anions in the voids were identified based on elemental analysis and charge neutrality considerations.

Single-crystal X-ray diffraction analysis revealed that all compounds crystallize in the orthorhombic *Pbca* space group (Table S1). The 2D layered structure is described using Eu complexes as a representative example (Fig. S1). PXRD and elemental analyses confirmed the crystalline phase purity of both complexes (details in the Experimental section and Fig. S3). The asymmetric unit of complex **1** contains one Bpydp ion, one BDC^{2-} ion, one Eu^{3+} ion, one coordinated water molecule, one free NO_3^- ion, and two free water molecules (Fig. S2a). The coordinated water molecule forms a hydrogen bond with a free water molecule in an adjacent unit, with an O-H···O distance of 2.464 Å and an O-H···O angle of 163.56°.

In the coordination framework, the Eu^{3+} ion acts as a critical node, being nine-coordinated by five oxygen atoms from three Bpydp ions, three oxygen atoms from two BDC^{2-} ions, and one oxygen atom from a water molecule, forming a two-dimensional (2D) coordination polymer. The Eu-O bond lengths range from 2.292 Å to 2.664 Å, and the O-Eu-O bond angles range from 49.51° to 155.3° (Tables S3, S5). Continuous shape measurement (CShM) gives a value of 2.277, indicating a coordination geometry similar to the Muffin configuration of Cs. The distance between pyridine rings in adjacent layers is 7.063 Å, indicating a weak π···π stacking interaction between the benzene ring of BDC^{2-} and the bipyridine rings, with negligible interactions between adjacent bipyridine rings.[1, 6]

Characterization

Powder X-ray diffraction (PXRD) was conducted using a Bruker-D8 diffractometer with Cu-Kα radiation. Fourier transform infrared (FTIR) spectra were recorded on a Perkin-Elmer Spectrum One spectrometer with KBr pellets. Electron spin resonance (ESR) measurements were taken using a Bruker EMXplus spectrometer. UV-vis diffuse reflectance spectra were obtained on a Lambda 900 instrument, using $BaSO_4$ as a reference. Emission spectra were collected with a Perkin Elmer FL6500 luminescence spectrophotometer.

A PLS-SXE300D 300W xenon lamp system fitted with a PLS-BP20365 (365 nm filter) was used for the photochromic studies. The sample was positioned 10 cm away from the xenon lamp. After being irradiated, the irradiated sample was used to record solid-state UV-vis diffuse reflectance and luminescence spectra.

The BET test was conducted using the Autosorb iQ from Quantachrome for full pore analysis, and the pore size distribution was analyzed using the BJH model. The TEM testing was conducted using the JEOL F200 from Japan Electron Optics Laboratory.

Computational details

All physical property calculations in this study were conducted using the Quickstep module in the CP2K package.[7] The cutoff energy (CUTOFF) was set to 1200 Ry, and the relative cutoff energy (REL_CUTOFF) was set to 70 Ry. Due to the large cell size, a 1×1×1 Monkhorst-Pack grid was used for the k-points. The DZVP-MOLOPT-SR-GTH basis set and GTH-PBE pseudopotentials were employed for all atoms. Geometry optimization was carried out using the Perdew-Burke-Ernzerhof (PBEsol) pure functional, while density of states (DOS) calculations on the optimized structures were performed using the PBE pure functional. The calculation data and free pore analysis of the crystal structure were both performed using Multiwfn 3.8 (dev).[8, 9]

Molecular orbital energy calculations were conducted using the Gaussian16 suite with structures optimized by CP2K.[10] Single-point energy evaluations were performed at the PBE0/6-311G(d) level for C, H, O, and N atoms and at the PBE0/MWB52 level for Eu atoms. Dispersion corrections were applied using BJ damping (keyword: empirical dispersion=gd3bj).

Supplementary Tables and Figures

Table S1. Crystallographic Data and Structural Refinements Parameters for **1** and **2**.

	1	**2**
Formula	$C_{24}H_{26}EuN_3O_{14}$	$C_{24}H_{26}TbN_3O_{14}$
*M*r (g·mol^{-1})	732.45	739.40
Temperature/K	293	150
Space group	*Pbca*	*Pbca*
Crystal system	orthorhombic	orthorhombic
a (Å)	14.0075(6)	14.6366(3)
b (Å)	19.7510(5)	18.5358(3)
c (Å)	20.4381(5)	19.7866(3)
α (°)	90	90
β (°)	90	90
γ (°)	90	90
V (Å^3)	5368.2(3)	5368.13(16)
Z	8	8
F (000)	2928	2944
Dc (gcm^{-3})	1.813	1.830
μ (mm^{-1})	17.429	13.658
R_{int}	0.0571	0.0763
	-12 ≤ h ≤ 16	−17 ≤ h ≤ 17
limiting indice	-13 ≤ k ≤ 22	−21 ≤ k ≤ 22
	-18 ≤ l ≤ 24	−23 ≤ l ≤ 23
Collected reflections	12662	55701
Unique reflections	4805	4917
GOF on F^2	1.031	1.042
R_1, wR_2 [I>2σ(I)]	0.0580 0.1464	0.0356 0.0820
R_1, wR_2 [all data]	0.0913 0.1695	0.0420 0.0959

$^a R_1 = \Sigma\, ||F_0| - |F_c|| / \Sigma\, |F_o|$. $^b wR_2 = \{\Sigma\, [w\,(F_0^2 - F_c^2)^2] / \Sigma\, w(F_0^2)^2\}^{1/2}$.

Table S2. The shortest donor-acceptor distances in **1** and **2**.

Complex	Donor	Acceptor	d(D···A)/Å
1	O2	N2	3.369
1	O7	N2	3.015
1	O6	N1	3.339
2	O1	N4	3.362
2	O14	N1	3.330
2	O4	N1	3.079

Table S3 Bond Lengths for **1**.

Atom	Atom	Length/Å
Eu1	O1	2.292(6)
Eu1	O3[1]	2.567(6)
Eu1	O4[1]	2.430(6)
Eu1	O5[2]	2.664(6)
Eu1	O5	2.388(6)
Eu1	O6[2]	2.525(7)
Eu1	O7[3]	2.511(7)
Eu1	O8[3]	2.436(7)
Eu1	O9	2.413(6)

[1]1-X,1/2+Y,1/2-Z; [2]1-X,1-Y,1-Z; [3]+X,1/2-Y, -1/2+Z

Table S4 Bond Lengths for **2**.

Atom	Atom	Length/Å
Tb1	O1	2.285(3)
Tb1	O4[1]	2.465(3)
Tb1	O6[2]	2.485(3)
Tb1	O8[2]	2.427(3)

Tb1	O10	2.258(3)
Tb1	O12[3]	2.350(3)
Tb1	O16[1]	2.398(3)
Tb1	O18	2.387(3)

[1]+X,3/2-Y,-1/2+Z; [2]1-X,-1/2+Y,1/2-Z; [3]1-X,1-Y,1-Z

Table S5 Bond Angles for **1.**

Atom	Atom	Atom	Angle/°	Atom	Atom	Atom	Angle/°
O1	Eu1	O3[1]	82.2(2)	O5	Eu1	O7[3]	82.9(2)
O1	Eu1	O4[1]	133.5(2)	O5	Eu1	O8[3]	82.1(2)
O1	Eu1	O5[2]	121.7(2)	O5	Eu1	O9	77.7(2)
O1	Eu1	O5	149.9(2)	O6[2]	Eu1	O3[1]	70.7(2)
O1	Eu1	O6[2]	82.0(2)	O6[2]	Eu1	O5[2]	49.51(18)
O1	Eu1	O7[3]	75.0(2)	O7[3]	Eu1	O3[1]	114.1(2)
O1	Eu1	O8[3]	99.7(2)	O7[3]	Eu1	O5[2]	139.91(18)
O1	Eu1	O9	77.7(2)	O7[3]	Eu1	O6[2]	155.3(2)
O3[1]	Eu1	O5[2]	104.7(2)	O8[3]	Eu1	O3[1]	72.6(2)
O4[1]	Eu1	O3[1]	52.02(17)	O8[3]	Eu1	O5[2]	138.1(2)
O4[1]	Eu1	O5[2]	70.60(19)	O8[3]	Eu1	O6[2]	142.7(2)
O4[1]	Eu1	O6[2]	75.9(2)	O8[3]	Eu1	O7[3]	52.5(2)
O4[1]	Eu1	O7[3]	127.0(2)	O9	Eu1	O3[1]	153.3(2)
O4[1]	Eu1	O8[3]	76.5(2)	O9	Eu1	O4[1]	140.9(2)
O5	Eu1	O3[1]	126.12(18)	O9	Eu1	O5[2]	72.2(2)
O5	Eu1	O4[1]	76.4(2)	O9	Eu1	O6[2]	89.1(2)
O5	Eu1	O5[2]	65.7(2)	O9	Eu1	O7[3]	77.5(2)
O5	Eu1	O6[2]	114.7(2)	O9	Eu1	O8[3]	127.9(2)

[1]1-X,1/2+Y,1/2-Z; [2]1-X,1-Y,1-Z; [3]+X,1/2-Y, -1/2+Z

Table S6 Bond Angles for **2.**

Atom	Atom	Atom	Angle/°	Atom	Atom	Atom	Angle/°
O1	Tb1	O4[1]	79.44(10)	O10	Tb1	O1	148.18(12)
O1	Tb1	O6[2]	129.23(10)	O10	Tb1	O4[1]	77.22(10)
O1	Tb1	O8[2]	76.84(11)	O10	Tb1	O6[2]	82.03(11)
O1	Tb1	O12[3]	106.88(11)	O10	Tb1	O8[2]	134.92(11)
O1	Tb1	O16[1]	88.01(11)	O10	Tb1	O12[3]	84.83(10)
O1	Tb1	O18	73.12(13)	O10	Tb1	O16[1]	95.21(11)
O4[1]	Tb1	O6[2]	122.95(10)	O10	Tb1	O18	81.74(14)
O8[2]	Tb1	O4[1]	128.23(11)	O16[1]	Tb1	O6[2]	76.60(11)
O8[2]	Tb1	O6[2]	53.12(9)	O16[1]	Tb1	O8[2]	80.10(11)
O12[3]	Tb1	O6[2]	75.15(12)	O18	Tb1	O4[1]	80.00(11)
O12[3]	Tb1	O8[2]	79.86(12)	O18	Tb1	O6[2]	147.68(11)
O12[3]	Tb1	O16[1]	151.46(12)	O18	Tb1	O8[2]	133.24(12)
O12[3]	Tb1	O18	75.70(13)	O18	Tb1	O16[1]	132.65(11)
O16[1]	Tb1	O4[1]	53.63(10)	O12[3]	Tb1	O4[1]	151.57(12)

[1]+X,3/2-Y,-1/2+Z; [2]1-X,-1/2+Y,1/2-Z; [3]1-X,1-Y,1-Z.

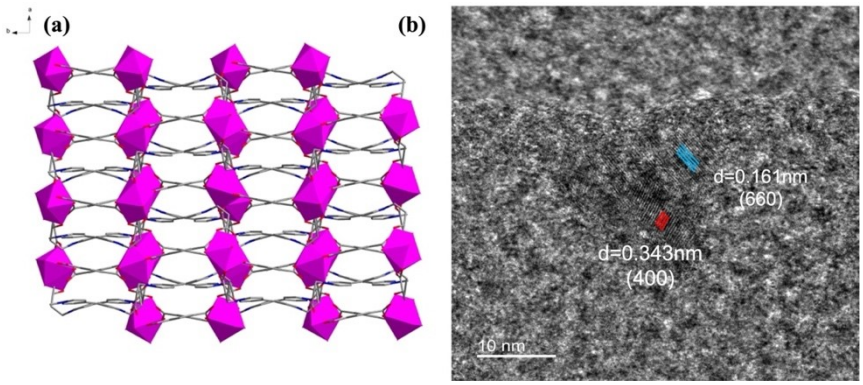

Fig. S1 (a) The two-dimensional (2D) CPs structure was constructed by linking rare earth ions and ligands through the terephthalic acid auxiliary ligand. (b) TEM image of complex **1**.

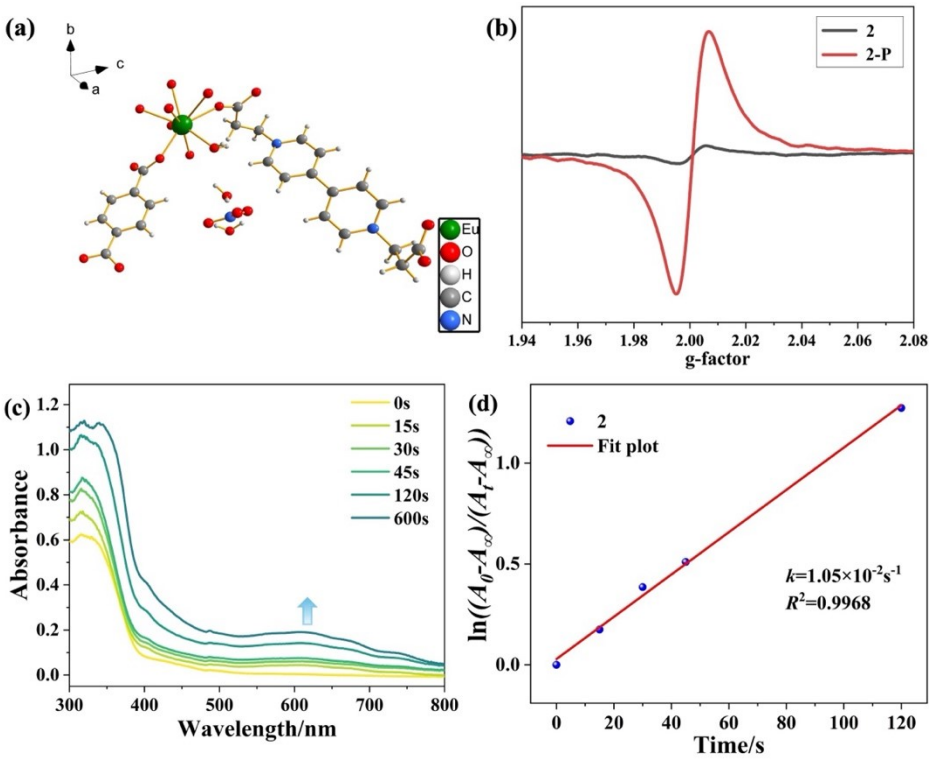

Fig. S2 (a) Asymmetric unit of complex **1**; (b) ESR spectra of **2** and **2-P**; (c) Changes in the UV-vis spectrum of **2** under 365 nm irradiation. (d) Photochemical reaction kinetics of **2** monitored at 604 nm.

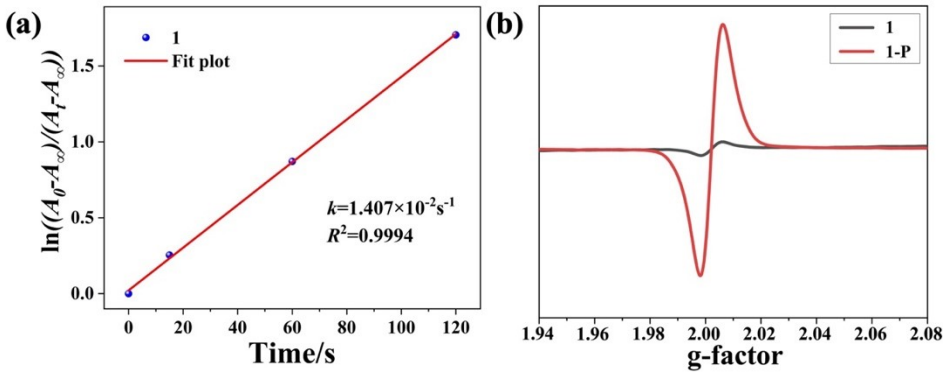

Fig. S3 (a) Photochemical reaction kinetics of **1** monitored at 610 nm. (b) ESR spectra of **1** and **1-P**.

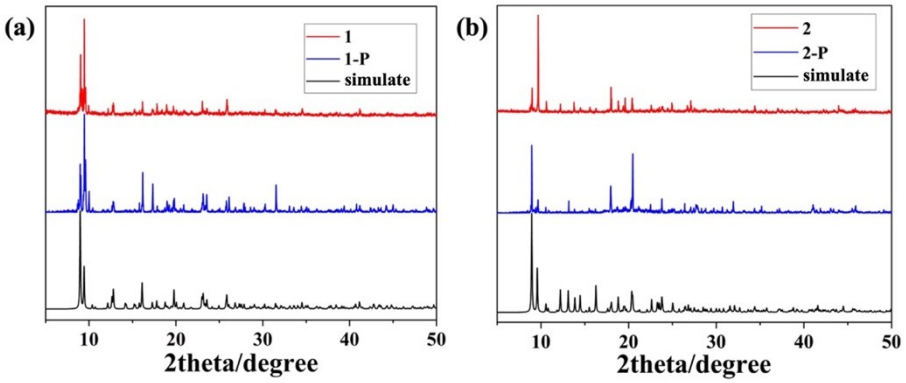

Fig. S4 PXRD spectra of **1** (a) and **2** (b) before and after irradiation.

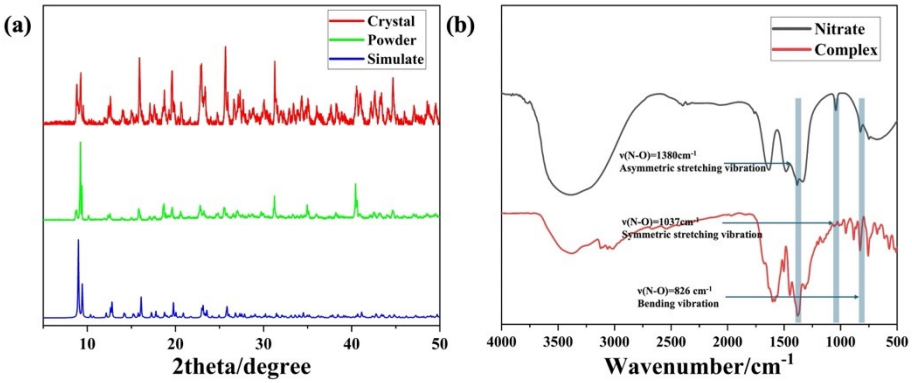

Fig. S5 (a) PXRD of complex **1** (crystal, powder, simulation); (b) Infrared spectrum of nitrate ions within the complex.

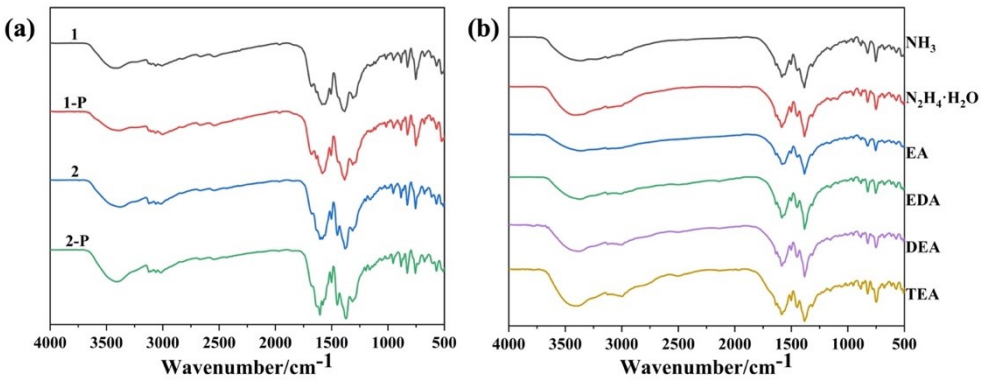

Fig. S6 (a) IR spectra of **1** and **2** before and after irradiation; (b) IR spectra of **1** after exposure to different volatile ammonia/amine vapors.

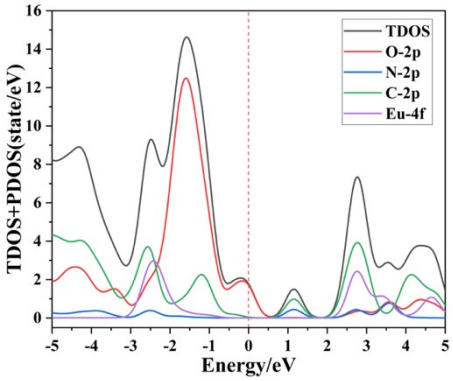

Fig. S7 TDOS and PDOS plots of **1**.

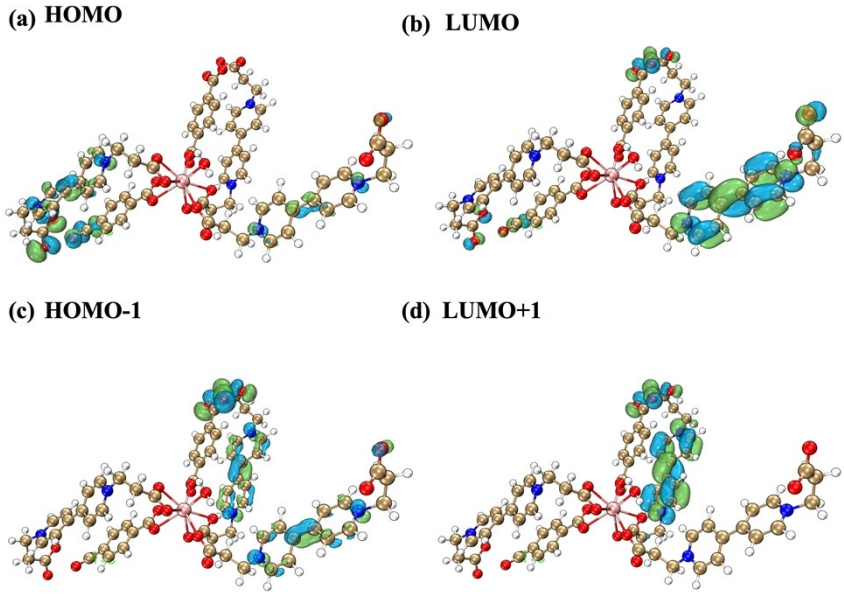

Fig. S8 HOMO (a), LUMO (b), HOMO-1 (c), and LUMO+1(d) profiles for **1**.

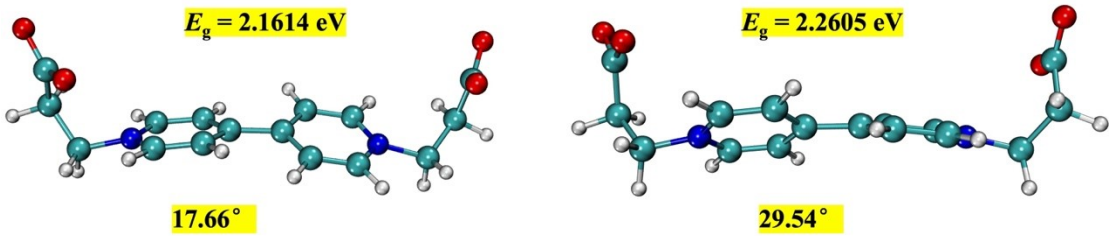

Fig. S9 The energy gaps of N, N'-4,4'-Bipyridinio-dipropionate ligands in Eu(left) and Tb(right) complexes at different dihedral angles.

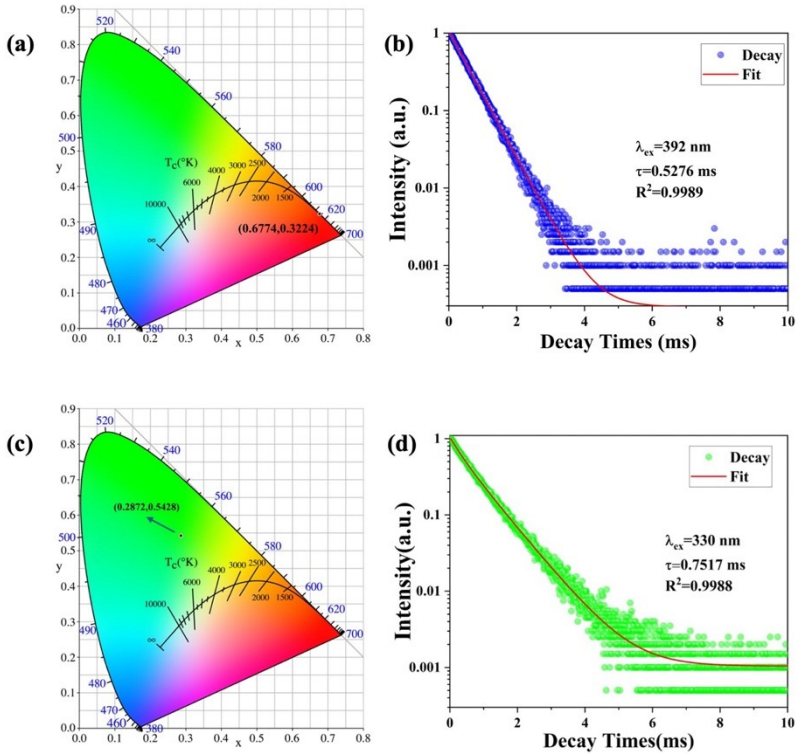

Fig. S10 (a) CIE chromaticity diagrams of **1**; (b) The fluorescence lifetime fitting of **1** under 370 nm excitation wavelength; (c) CIE chromaticity diagrams of **2**; (d) The fluorescence lifetime fitting of **2** under 330 nm excitation wavelength.

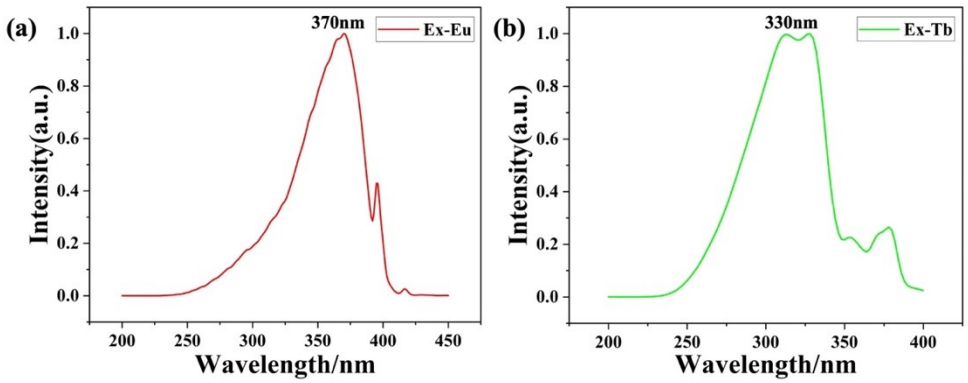

Fig. S11 Fluorescence Excitation Spectra of **1**(a) and **2**(b).

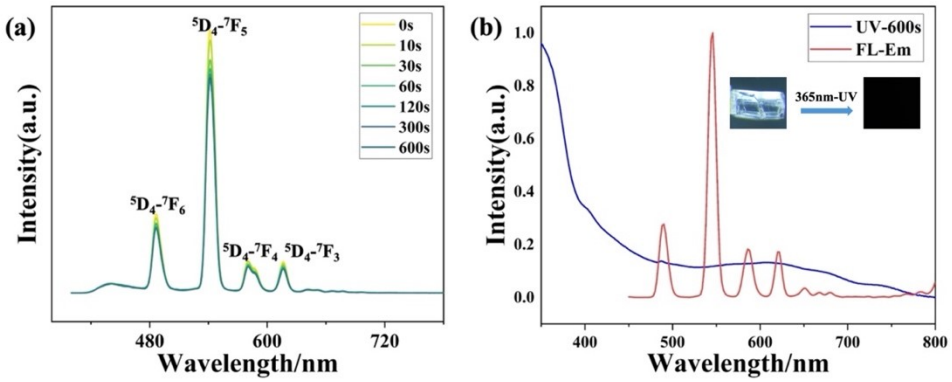

Fig. S12 Time-dependent fluorescence intensity plot of **2** under 365 nm irradiation; (b) Overlapping regions in the UV-vis and Fluorescence spectra of **2**. (Inset: Crystal fluorescence before and after UV irradiation.)

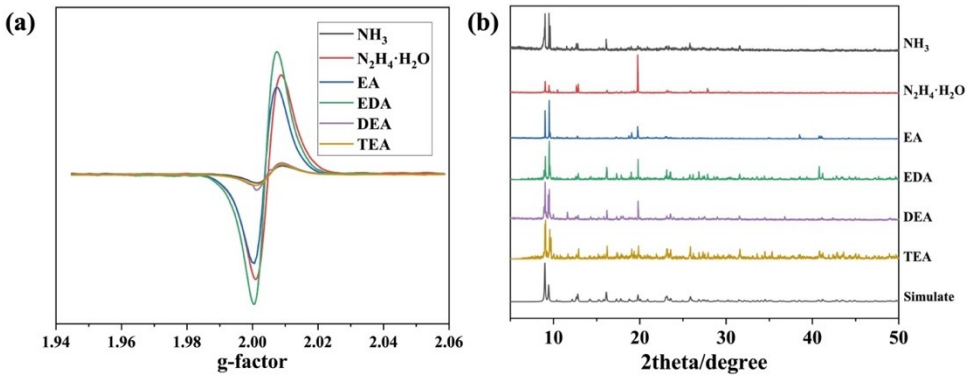

Fig. S13 (a) ESR spectra of **1** after exposure to different volatile ammonia/amine vapors; (b) PXRD spectra of **1** after exposure to different volatile ammonia/amine vapors.

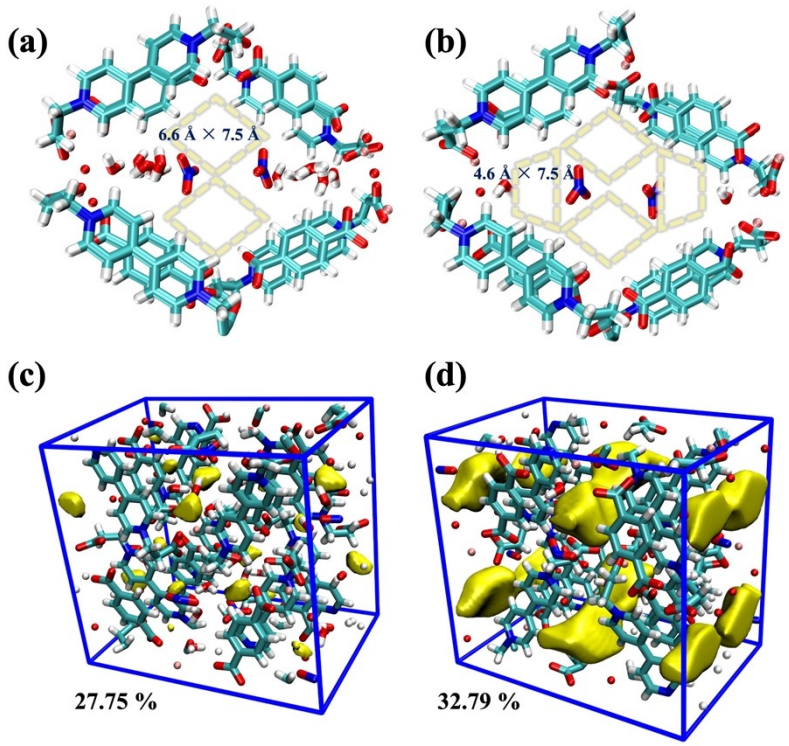

Fig. S14 (a) The crystal structure and pore size of **1**; (b) changes in pore size after removing water molecules; (c) visualization of the free volume of the crystal unit; (d) free volume after removing water molecules. (Calculated using Multiwfn 3.8 (dev) and VMD 1.9.4)

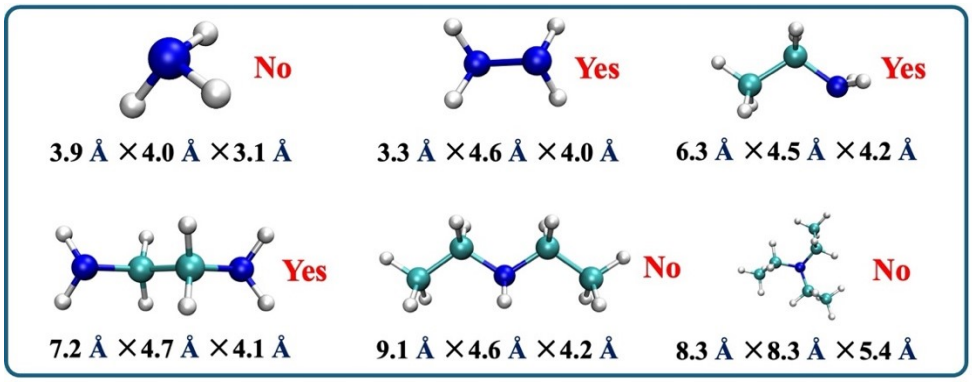

Fig. S15 The dimensions of various amine molecules were calculated using Multiwfn 3.8 (dev).

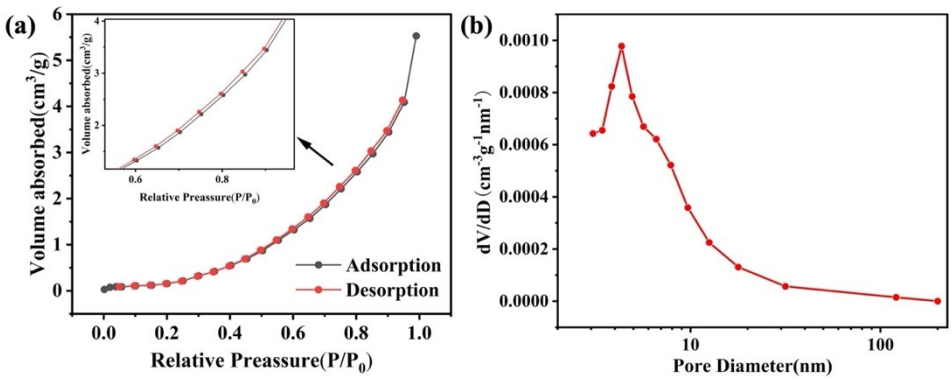

Fig. S16 (a) Nitrogen adsorption-desorption isotherms of complex **1**; (b) Pore size distribution curve fitted using the BJH model.

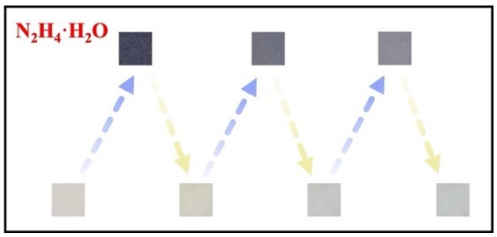

Fig. S17 Fatigue testing of amine test paper for detecting $N_2H_4 \cdot H_2O$ (hydrazine hydrate).

References:

1. T. Zhou, J. Chen, T. Wang, H. Yan, Y. Xu, Y. Li and W. Sun, *ACS Appl. Mater. Interfaces*, 2022, **14**, 57037-57046.
2. C. Sun, G. Xu, X.-M. Jiang, G.-E. Wang, P.-Y. Guo, M.-S. Wang and G.-C. Guo, *J. Am. Chem. Soc.*, 2018, **140**, 2805-2811.
3. L. J. Bourhis, O. V. Dolomanov, R. J. Gildea, J. A. K. Howard and H. Puschmann, *Acta Crystallogr. Sect. A*, 2015, **71**, 59-75.
4. O. V. Dolomanov, L. J. Bourhis, R. J. Gildea, J. A. K. Howard and H. Puschmann, *J. Appl. Crystallogr.*, 2009, **42**, 339-341.
5. G. M. Sheldrick, *Acta Crystallogr. Sect. C-Struct. Chem.*, 2015, **71**, 3-8.
6. D.-D. Yang, Y.-S. Shi, T. Xiao, Y.-H. Fang and X.-J. Zheng, *Inorg. Chem.*, 2023, **62**, 6084-6091.
7. T. D. Kühne, M. Iannuzzi, M. Del Ben, V. V. Rybkin, P. Seewald, F. Stein, T. Laino, R. Z. Khaliullin, O. Schütt, F. Schiffmann, D. Golze, J. Wilhelm, S. Chulkov, M. H. Bani-Hashemian, V. Weber, U. Borštnik, M. Taillefumier, A. S. Jakobovits, A. Lazzaro, H. Pabst, T. Müller, R. Schade, M. Guidon, S. Andermatt, N. Holmberg, G. K. Schenter, A. Hehn, A. Bussy, F. Belleflamme, G. Tabacchi, A. Glöß, M. Lass, I. Bethune, C. J. Mundy, C. Plessl, M. Watkins, J. VandeVondele, M. Krack and J. Hutter, *The Journal of Chemical Physics*, 2020, **152**, 194103.
8. T. Lu and F. Chen, *J. Comput. Chem.*, 2012, **33**, 580-592.
9. Z. Liu, T. Lu and Q. Chen, *Carbon*, 2020, **165**, 461-467.
10. M. J. Frisch, G. W. Trucks, H. B. Schlegel, G. E. Scuseria, M. A. Robb, J. R. Cheeseman, G. Scalmani, V. Barone, G. A. Petersson, H. Nakatsuji, X. Li, M. Caricato, A. V. Marenich, J. Bloino, B. G. Janesko, R. Gomperts, B. Mennucci, H. P. Hratchian, J. V. Ortiz, A. F. Izmaylov, J. L. Sonnenberg, D. Williams-Young, F. Ding, F. Lipparini, F. Egidi, J. Goings, B. Peng, A. Petrone, T. Henderson, D. Ranasinghe, V. G. Zakrzewski, J. Gao, N. Rega, G. Zheng, W. Liang, M. Hada, M. Ehara, K. Toyota, R. Fukuda, J. Hasegawa, M. Ishida, T. Nakajima, Y. Honda, O. Kitao, H. Nakai, T. Vreven, K. Throssell, J. A. Montgomery Jr., J. E. Peralta, F. Ogliaro, M. J. Bearpark, J. J. Heyd, E. N. Brothers, K. N. Kudin, V. N. Staroverov, T. A. Keith, R. Kobayashi, J. Normand, K. Raghavachari, A. P. Rendell, J. C. Burant, S. S. Iyengar, J. Tomasi, M. Cossi, J. M. Millam, M. Klene, C. Adamo, R. Cammi, J. W. Ochterski, R. L. Martin, K. Morokuma, O. Farkas, J. B. Foresman and D. J. Fox, *Journal*, 2016.